JACS
JOURNAL OF THE AMERICAN CHEMICAL SOCIETY
Article
pubs.acs.org/JACS

Cerium Photosensitizers: Structure–Function Relationships and Applications in Photocatalytic Aryl Coupling Reactions

Haolin Yin, Patrick J. Carroll, Brian C. Manor, Jessica M. Anna,* and Eric J. Schelter*

P. Roy and Diana T. Vagelos Laboratories, Department of Chemistry, University of Pennsylvania, 231 South 34 Street, Philadelphia, Pennsylvania 19104, United States

Supporting Information

ABSTRACT: Two complete mixed-ligand series of luminescent Ce^{III} complexes with the general formulas $[(Me_3Si)_2NC(N^iPr)_2]_xCe^{III}[N(SiMe_3)_2]_{3-x}$ (x = 0, **1-N**; x = 1, **2-N**, x = 2, **3-N**; x = 3, **4**) and $[(Me_3Si)_2NC(N^iPr)_2]_xCe^{III}(OAr)_{3-x}$ (x = 0, **1-OAr**; x = 1, **2-OAr**, x = 2, **3-OAr**; x = 3, **4**) were developed, featuring photoluminescence quantum yields up to 0.81(2) and lifetimes to 117(1) ns. Although the 4f → 5d absorptive transitions for these complexes were all found at ca. 420 nm, their emission bands exhibited large Stokes shifts with maxima occurring at 553 nm for **1-N**, 518 nm for **2-N**, 508 nm for **3-N**, and 459 nm for **4**, featuring yellow, lime-green, green, and blue light, respectively. Combined time-dependent density functional theory (TD-DFT) calculations and spectroscopic studies suggested that the long-lived ^2D excited states of these complexes corresponded to singly occupied $5d_{z^2}$ orbitals. The observed difference in the Stokes shifts was attributed to the relaxation of excited states through vibrational processes facilitated by the ligands. The photochemistry of the sterically congested complex **4** was demonstrated by C–C bond forming reaction between 4-fluoroiodobenzene and benzene through an outer sphere electron transfer pathway, which expands the capabilities of cerium photosensitizers beyond our previous results that demonstrated inner sphere halogen atom abstraction reactivity by **1-N**.

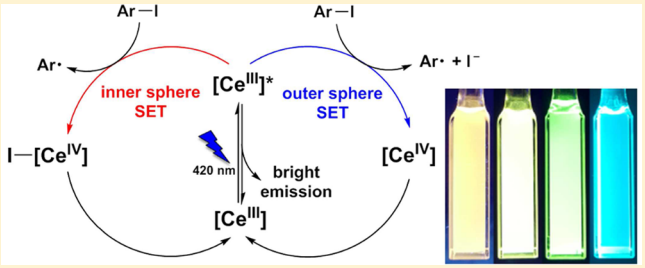

1. INTRODUCTION

Photoluminescent complexes find direct applications in light-emitting materials,[1] but have also drawn significant attention for applications in photovoltaic devices[2,3] and photoredox catalysis.[4] The luminescence phenomenon implies the existence of long-lived electronic excited states that are energetically poised to engage in single electron transfer (SET) reactions, much more so than in their ground states. The development of photoreduction chemistry relies on the availability of powerful photoreductants as well as the ability to tune their optical and electrochemical properties using simple modifications.[5−7] Molecular complexes, including $Ru(bpy)_3^{2+}$ (bpy = 2,2′-bipyridine), *fac*-$Ir(ppy)_3$ (ppy = 2,2′-phenylpyridine), and their derivatives, have been widely applied as visible light photoredox catalysts to promote C–C bond forming reactions[8−18] and CO_2 reduction.[19] Similarly, dimeric $[Au_2(\mu\text{-dppm})_2]^{2+}$ (dppm = bis(diphenylphosphanyl)methane) was also shown to promote C–C bond formation under UV light or sunlight.[20,21] As powerful reductants with excited-state reduction potentials as low as −3.0 V versus $Cp_2Fe^{0/+}$, the excited states of luminescent tungsten(0) isocyanide complexes were shown to be effectively quenched by very weak oxidants such as benzophenone and anthracene.[22,23] Moreover, developments in C–N,[24−26] C–O,[27] C–S,[28] and C–C[29−31] bond coupling reactions with luminescent Cu^I complexes indicate that SET mechanisms are viable pathways for Ullmann-type coupling chemistry. And the use of Cu^I photosensitizers has contributed to establishing the application of earth abundant elements for photoredox catalysis.[32−35]

Single photon excitation of transition metal photosensitizers leads to excited states through metal-to-ligand charge transfer transitions (MLCT).[36] The resulting singlet excited states quickly undergo intersystem crossing (ISC) to afford long-lived triplet states. In order to take full advantage of solar energy, the ideal absorption energy for visible light photosensitizers is ca. 2.8 eV (440 nm, blue light), defined by the intensity maximum in the sunlight spectrum.[4,37,38] However, the intersystem crossing (ISC) process inevitably results in losses of absorbed energy.

In contrast to the transition metal photosensitizers, the luminescence of the Ce^{III} cation is metal-centered and does not involve a change in spin state.[39,40] The interconfigurational f → d transition for Ce^{III} cations is electron dipole allowed based on $\Delta S = 0$ and $|J - J'| \leq 3 \leq |J + J'|$ selection rules, where J and J' are the total angular momentum quantum numbers of the f^n ground and $f^{n-1}d^1$ excited-state configurations, respectively.[41] The promise of applying Ce^{III} cations for photochemistry was supported by early photolysis studies in aqueous solutions; H_2 gas evolution was observed upon irradiation of aqueous solutions containing Ce^{III} cations with UV light.[42−45] Recently, we reported a physical basis for visible light promoted reductive

Received: March 2, 2016
Published: April 8, 2016

DOI: 10.1021/jacs.6b02248
J. Am. Chem. Soc. 2016, 138, 5984−5993

photochemistry in organic media with well-defined molecular complexes, $Ce[N(SiMe_3)_2]_3$ (**1-N**) and $[(Me_3Si)_2NC(N^iPr)_2]$-$Ce[N(SiMe_3)_2]_2$ (**2-N**).[46] Both complexes absorbed blue light to access ^2D excited states[47] featuring singly occupied $5d_{z^2}$ orbitals. The metalloradical character of the resulting ^2D excited states promoted inner sphere halogen atom abstraction reactions toward $PhCH_2Cl$, aryl iodides, and aryl bromides in stoichiometric and catalytic fashions. These photoreduction reactivities demonstrated that the energy of light absorbed by these complexes can be effectively directed into chemical transformations.

Our interests in developing Ce^{III} photosensitizers are also grounded in the earth abundance of the element. Cerium has a similar abundance to copper in Earth's upper continental crust with relative abundance of $\sim 10^{1.5}$ (atoms per 10^6 atoms of Si) and is more abundant than tungsten (10^0), gold (10^{-3}), ruthenium (10^{-3}), and iridium ($<10^{-5}$), respectively.[48] Cerium is also readily separated from other lanthanide elements using oxidation chemistry[49] and is a waste byproduct in the separations chemistry of light rare earth elements.

Solid materials doped with Ce^{3+} cations were important in the development of white light LEDs due to their broad emission bands originating from the ^2D excited states of Ce^{3+} cations.[50] For example, the yellow emitter YAG:Ce^{3+} absorbs blue light and exhibits a broad emission band spanning from 450 nm to over 700 nm.[51] Thus, the combination of emitted light from YAG:Ce phosphor and transmitted blue light from blue LEDs produces white light. Although Ce^{III} cations exhibit intrinsic 4f → 5d absorptive transitions,[52] luminescence has not typically been observed from molecular Ce^{III} compounds likely due to rapid quenching of their excited states by nonradiative relaxation pathways.[39] In fact, only a small number of luminescent molecular Ce^{III} complexes have been reported.[52−58] Among these, a large variation was observed in the luminescence properties; a photoluminescence quantum yield of 0.7 was reported for $[K(THF)_2][(C_5Me_5)_2CeI_2]$ compared to 0.01 for $[(C_5Me_5)_2CeI(NCMe)_2]$.[54] In order to rationally design Ce^{III} photosensitizers for varied purposes, a working model of the photophysical properties of Ce^{III} luminescence is required.[59] Herein, we report two complete mixed-ligand series of cerium(III) complexes that display varied emission wavelengths corresponding to yellow, green, and blue light, despite basically invariant absorption bands at ca. 420 nm. The photophysical properties and excited-state reduction potentials of the series were evaluated based on electrochemical and spectroscopic data. We also demonstrate that a sterically congested homoleptic tris-guanidinate Ce^{III} complex (**4**) can be applied as photocatalyst by outer sphere electron transfer, a fundamental expansion from the exclusively inner sphere photosensitizers demonstrated in our initial report.[46]

2. RESULTS AND DISCUSSION

2.1. Synthesis of Luminescent Cerium Complexes. The promise of applying rigid guanidinate ligands toward accessing highly luminescent Ce(III) complexes was initiated from a simple insertion reaction of $Ce[N(SiMe_3)_2]_3$ (**1-N**) with excess *N,N′*-diisopropylcarbodiimide (Scheme 1).[46] The resulting monoinsertion product $[(Me_3Si)_2NC(N^iPr)_2]Ce[N(SiMe_3)_2]_2$ (**2-N**) was found to be a much brighter emitter than **1-N**; the photoluminescence quantum yields (Φ_{PL}) were determined to be 0.46 for **2-N** compared to 0.03 for **1-N**.[46] To extend the scope of luminescent complexes, the corresponding aryloxide complex, $[(Me_3Si)_2NC(N^iPr)_2]Ce(OAr)_2$ (**2-OAr**), was synthesized through protonolysis reaction of **2-N** with 2 equiv of HOAr (Ar = 2,6-di-*tert*-butylphenol) (Scheme 1). Similarly, protonolysis of **1-N** with 3 equiv of HOAr resulted in $Ce(OAr)_3$ (**1-OAr**) according to a previous report.[60,61]

Scheme 1. Synthesis of Luminescent Ce(III) Complexes

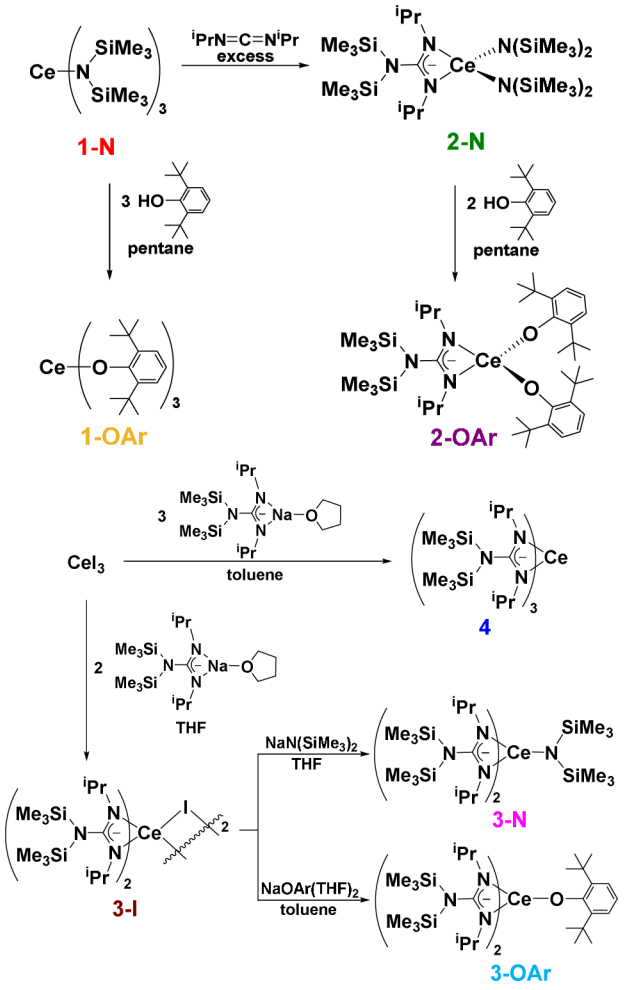

With the monoguanidinate bis-amide/aryloxide Ce(III) complexes in hand, we set out to prepare bis- and tris-guanidinate derivatives. However, treatment of **2-N** with excess *N,N′*-diisopropylcarbodiimide did not lead to further insertion reactivity up to 80 °C in benzene.[46] In order to understand the energy requirements for the insertion reactions, density functional theory (DFT) calculations were carried out for **1-N** and the established and expected insertion products: **2-N**, $[(Me_3Si)_2NC(N^iPr)_2]_2Ce[N(SiMe_3)_2]$ (**3-N**), and $[(Me_3Si)_2NC(N^iPr)_2]_3Ce$ (**4**) in the gas phase at the B3LYP level of theory. The results from the ground-state DFT calculations were consistent with experimental observations; ΔG_1 at 298.15 K for the first carbodiimide insertion into **1-N** was found to be essentially thermoneutral (0.79 kcal mol^{-1}) while the second and third insertions were less favorable on thermodynamic grounds (ΔG_2 = 3.87 kcal mol^{-1}, ΔG_3 = 8.46 kcal mol^{-1}) (Figure S83).

In light of these observations, salt metathesis reactions were performed between CeI_3 and 2 equiv of $[(Me_3Si)_2NC(N^iPr)_2]$-Na(THF) in THF to afford the pale yellow bridging iodide complex, $[(Me_3Si)_2NC(N^iPr)_2]_2Ce^{III}\}_2(\mu^2\text{-}I)_2$ (**3-I**) (Scheme 1). An X-ray crystallography study revealed the dimeric structure of the product, featuring a $[Ce_2I_2]^{4+}$ diamondoid

DOI: 10.1021/jacs.6b02248
J. Am. Chem. Soc. 2016, 138, 5984−5993

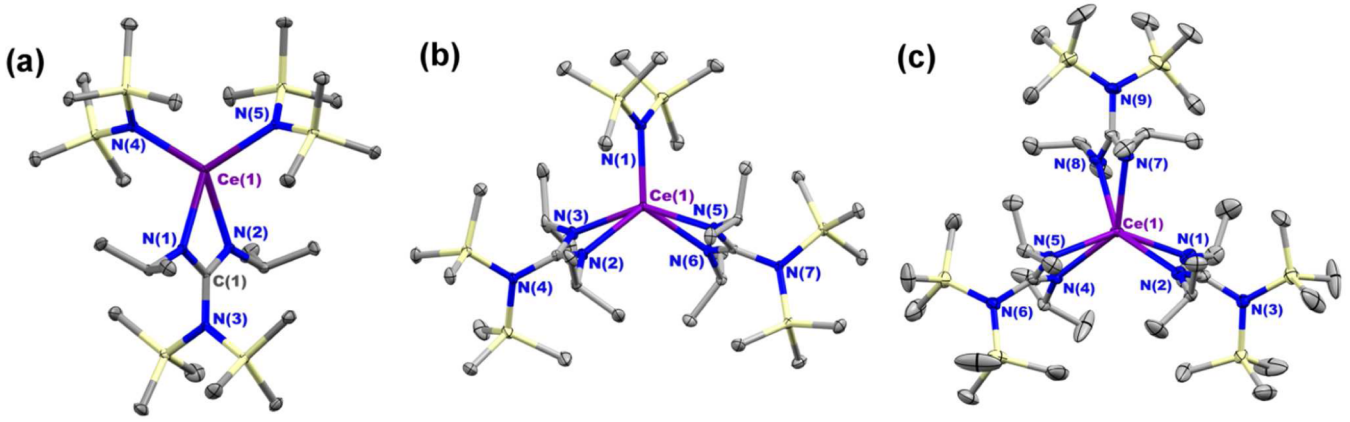

Figure 1. Thermal ellipsoid plots of **2-N** (a), **3-N** (b), and **4** (c) at the 30% probability level.

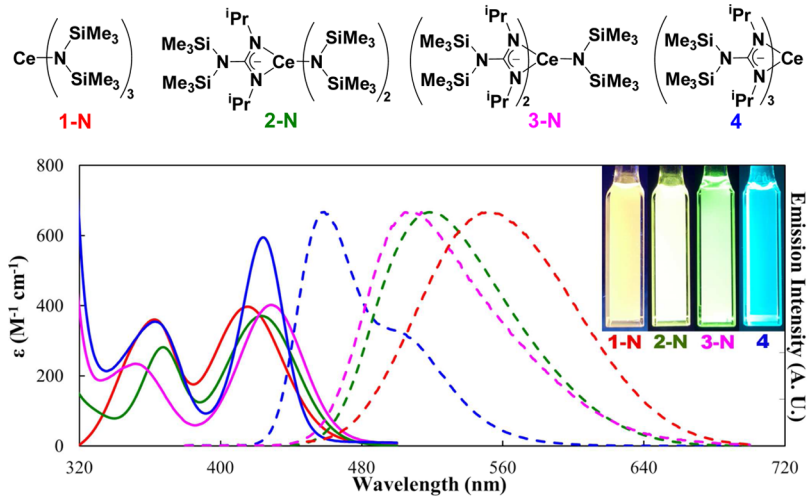

Figure 2. Absorption (solid lines) and emission spectra (dashed lines) of **1-N** (red), **2-N** (green), **3-N** (pink), and **4** (blue). Inset: images of toluene solution of **1-N**, **2-N**, **3-N**, and **4** in 1 cm path length quartz cuvettes (1.0 mM) under 365 nm UV irradiation.

core (Figure S2). Four broad resonances were observed in the ^{1}H NMR spectrum obtained at 300 K for **3-I** in toluene-d_8 or C_6D_6 (Figure S11). Heating the toluene-d_8 solution of **3-I** resulted in peak coalescence at 325 K (Figure S13). The ^{1}H NMR spectrum, fully resolved at 380 K (Figure S12), displayed three resonances at 14.20, 3.68, and −3.26 ppm in a 2:18:12 ratio, attributable to −CH(^{i}Pr), −CH$_3$(^{i}Pr), and −CH$_3$(SiMe$_3$) groups, respectively, from the guanidinate ligands. Further salt metathesis reactions of **3-I** with NaN(SiMe$_3$)$_2$ or Na(OAr)(THF)$_2$ afforded bright yellow solids of corresponding amide and aryloxide derivatives, [(Me$_3$Si)$_2$NC(N^{i}Pr)$_2$]$_2$Ce[N(SiMe$_3$)$_2$] (**3-N**) and [(Me$_3$Si)$_2$NC(N^{i}Pr)$_2$]$_2$Ce(OAr) (**3-OAr**) (Scheme 1).

Conversely, treatment of CeI$_3$ with 3 equiv of [(Me$_3$Si)$_2$NC(N^{i}Pr)$_2$]Na(THF) in toluene afforded pale yellow solids of [(Me$_3$Si)$_2$NC(N^{i}Pr)$_2$]$_3$Ce (**4**) (Scheme 1). The identity of **4** was confirmed by X-ray crystallography (Figure 1c), constituting the first homoleptic Ce^{III} guanidinate complex. The ^{1}H NMR spectrum of **4** in C_6D_6 at 300 K revealed three resonances at 10.02, 2.81, and −4.15 ppm, consistent with a C_{3v} solution geometry. Complex **4** was robust toward ligand redistribution reactions; heating a 1:1 mixture of **1-N** and **4** in C_6D_6 at 80 °C for 30 h resulted in only negligible amounts of **2-N** and **3-N** as detected by ^{1}H NMR spectroscopy (Figure S21). The preparation of the yellow Ce^{III} compounds described above completed two mixed-ligand series with the general formulas [(Me$_3$Si)$_2$NC(N^{i}Pr)$_2$]$_x$Ce^{III}[N(SiMe$_3$)$_2$]$_{3-x}$ (x = 0, **1-N**; x = 1, **2-N**, x = 2, **3-N**; x = 3, **4**) and [(Me$_3$Si)$_2$NC(N^{i}Pr)$_2$]$_x$Ce^{III}(OAr)$_{3-x}$ (x = 0, **1-OAr**; x = 1, **2-OAr**, x = 2, **3-OAr**; x = 3, **4**). All of these compounds were found to be luminescent, thus allowing a systematic comparison by stepwise structural variations to study the photophysical properties of luminescent Ce^{III} complexes.

2.2. Electronic Structures of Luminescent Ce(III) Complexes. We noted that both series of Ce^{III} complexes defined in the current work were exclusively yellow despite the difference in their ligand coordination spheres. Indeed, the electronic absorption spectra collected for **1-N**, **2-N**, **3-N**, **4**, and **3-OAr**, **2-OAr**, and **1-OAr** in toluene displayed remarkable similarity; absorption features at ca. 420 nm and ca. 360 nm were observed for all complexes with absorptivities of $\varepsilon \sim 10^2$ M^{-1} cm^{-1}. These molar extinction coefficients are consistent with reported values for f → d transitions.[62,63] Absorption and emission spectra for the representative guanidinate−amide mixed-ligand series are shown in Figure 2, featuring the yellow-emitting complex **1-N**, lime-green **2-N**, green **3-N**, and blue **4**.

Our previous work on **1-N** and **2-N** showed the origins of the absorption features between 320 and 500 nm as metal-centered interconfigurational 4f → 5d transitions.[46] For the other members of the series, **3-N** and **4**, time-dependent

DOI: 10.1021/jacs.6b02248
J. Am. Chem. Soc. 2016, 138, 5984−5993

density functional theory (TD-DFT) calculations were carried out at the B3LYP level of theory to assist in assignment of the observed transitions. Subsequent to the TD-DFT calculations, natural transition orbital (NTO) computations were performed to visualize compact orbital representations for the vertical excitations of interest.[64,65]

For all the complexes, the donor and acceptor orbitals for the transition at ca. 420 nm were identified to be 4f orbitals and $5d_{z^2}$ orbitals, respectively (Figure 3). This result was readily

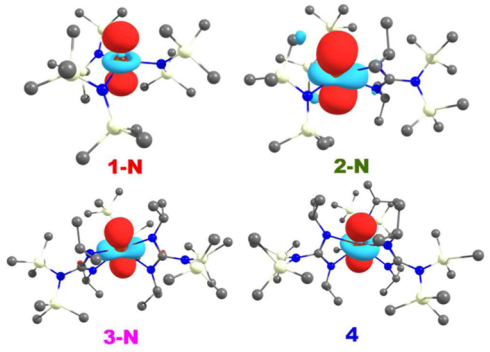

Figure 3. Calculated acceptor natural transition orbitals (NTOs) of the transition at ca. 420 nm for **1-N**, **2-N**, **3-N**, and **4**, demonstrating the primarily nonbonding $5d_{z^2}$ orbital character.

rationalized by inspection of the complex crystal structures. In the complexes with approximately C_{3v} geometry (**1-N** and **4**), or those with approximately C_{2v} geometry (**2-N** and **3-N**), the $5d_{z^2}$ orbitals are essentially nonbonding in character. While the ligand field has an only small impact on the optical energies of 4f orbitals,[66] the energy of metal-centered 4f → 5d transitions is dependent on the relative energies of the acceptor 5d orbitals.[67] Therefore, the nonbonding nature of the $5d_{z^2}$ orbitals is understood to be responsible for the similar lowest energy absorption features in visible range (400−800 nm) of these luminescent Ce^{III} complexes, as well as their yellow colors.

On the other hand, the identities of acceptor orbitals for the second lowest energy absorptive 4f → 5d transitions are dictated by the ligand field splitting of the 5d manifold. For **1-N** and **4** with C_{3v} solution symmetry, 2-fold degenerate sets of 5d orbitals were assigned as the corresponding acceptor orbitals using NTO calculations (Figures S81 and S82). In comparison, the degeneracy of the 5d manifold was broken for complexes **2-N** and **3-N** in approximate C_{2v} solution symmetry; only one of the $5d_{xz}$ or $5d_{yz}$ orbitals was identified as the acceptor (Figure S77).

The TD-DFT assignment of the absorptive transitions was further supported by experimental evidence. The lanthanum analogue of **1-N**, $La[N(SiMe_3)_2]_3$ ($4f^0$), showed no absorption feature between 320 and 500 nm, further supporting that both absorption bands observed for **1-N** are 4f → 5d transitions and not CT transitions (Figure S42). We also prepared the NEt_4Cl adduct of **1-N**. The blue-emitting compound, $[NEt_4]\{Ce^{III}Cl[N(SiMe_3)_2]_3\}$ (**1-NCl**$^-$), demonstrated a trigonal pyramidal $CeClN_3$ core with sum of N−Ce−N angles at 347.3(1)° (Figure S8). The electronic absorption spectrum of **1-NCl**$^-$ demonstrated only one absorption feature at 366 nm as compared to two bands for **1-N** (Figure S42). The absence of the absorptive transition at ca. 420 nm for **1-NCl**$^-$ is consistent with the assignment as a transition to a state corresponding to the $5d_{z^2}$ orbital in **1-N** that is driven to higher energies by crystal field arguments upon coordination of Cl^- in **1-NCl**$^-$.

Despite the similar absorption energies for **1-N**, **2-N**, **3-N**, and **4**, the wavelengths of their emission maxima spanned a large range from 553 nm (**1-N**) to 459 nm (**4**) (Figure 2). This observation was best described with the observed Stokes shifts calculated from the difference in wavelength between the positions of emission maxima and the lowest energy absorption maxima. Among the guanidinate−amide mixed-ligand series, complex **1-N** featured the largest Stokes shift of 138 nm while complex **4** demonstrated a much smaller Stokes shift of 35 nm. Interestingly, the observed Stokes shifts were found to decrease with increasing numbers of guanidinate ligands across the series (Figure 4, solid line). The existence of such a trend was

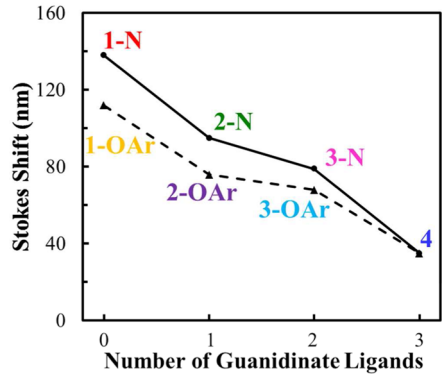

Figure 4. Observed Stokes shift of guanidinate−amide mixed-ligand series (solid line, including **1-N**, **2-N**, **3-N**, and **4**) and guanidinate−aryloxide mixed-ligand series (dashed line, including **1-OAr**, **2-OAr**, **3-OAr**, and **4**).

confirmed by the guanidinate−aryloxide mixed-ligand series (Figure 4, dashed line). The largest Stokes shift in the guanidinate−aryloxide mixed-ligand series was found to be 112 nm for **1-OAr**, smaller than 138 nm observed for **1-N**.

In an effort to understand the Stokes shifts, we attempted to assign the ground and excited states giving rise to the emissive transitions. We determined that the lifetime for **4** was invariant when measured at different emission wavelengths. This result suggested that only one long-lived excited state was involved in the emission process. Excitation spectra collected in toluene for both series of complexes showed intense bands, overlapping with their lowest energy absorption bands at ca. 420 nm (See Figures S44−S51). This observation allowed us to conclude that lowest lying $5d_{z^2}$ orbital based excited state corresponded to the long-lived excited state for these complexes. All the emission spectra were fit with two overlapping Gaussian functions (on an energy scale) separated by 1200 to 1700 cm^{-1} (Figures S52−S59). The energy difference between the two Gaussian functions was consistent with the spin−orbit splitting the ^2F ground-state manifold into the $^2F_{5/2}$ ground state and $^2F_{7/2}$ excited state for the Ce^{3+} cation.

The Stokes shifts represent the degree of energy loss between excited state following the absorptive vertical transition and long-lived excited state. Since complexes **1-N**, **2-N**, **3-N**, and **4** demonstrated a common long-lived ^2D excited state with singly occupied nonbonding $5d_{z^2}$ orbital and 4f orbital based ground states, very little geometric change was expected for the excited-state structures compared to the ground-state ones. This was consistent with the findings for

DOI: 10.1021/jacs.6b02248
J. Am. Chem. Soc. 2016, 138, 5984−5993

reported complexes $[(C_5H_4SiMe_3)_3Ln^{II}]^-$ (Ln = La, Ce, Pr, Nd, Gd, Tb, Dy, Ho, Er)[68−70] with $5d_{z^2}$ orbital based ground states and $[(C_5H_4SiMe_3)_3U^{II}]^-$[71] and $\{[C_5H_3(SiMe_3)_2]_3Th^{II}\}^-$[68] with $6d_{z^2}$ orbital based ground states; the bond lengths and geometries of these divalent species were essentially identical compared to their Ln^{III}, U^{III}, and Th^{III} counterparts, resulting from the nonbonding character of $5d_{z^2}$ and $6d_{z^2}$ orbitals.

The difference in the Stokes shifts for the guanidinate−amide and guanidinate−aryloxide series reflects the difference in energy relaxation of long-lived ^{2}D excited states in the series. Such decrease of relaxed excited-state energy is likely facilitated by coupled vibrational modes. We expected that the dominant relaxation pathway occurred through interactions of the metal cation with ligand C−H oscillators. The geometry of complex **1-N** had previously been determined to be trigonal pyramidal through gas phase electron diffraction studies.[72] The deviation of **1-N** from trigonal planar geometry implied the presence of C−H agostic interactions between the Ce^{3+} cation and methyl groups of the silyl amide ligands. The replacement of amide ligands with guanidinate ligands removed C−H agostic interactions and thus resulted in less dissipation of energy through vibrational process in excited state. In addition, we postulate that the rigidity of bidentate guanidinate ligands compared to monodentate amide ligands restricted the vibration relaxation process through Ce−N and N−Si bonds.

To quantitatively determine the efficiency of emission, photoluminescence quantum yields (Φ_{PL}) were obtained in toluene through a comparative method[73] referenced to 9,10-diphenylanthracene (Φ_{std} = 0.97) in cyclohexane.[74] The calculated quantum yields (Figure 5) were found to increase

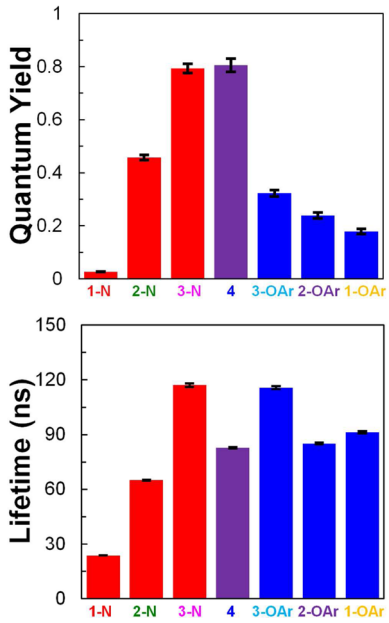

Figure 5. Quantum yields and lifetime data for **1-N**, **2-N**, **3-N**, **4**, **3-OAr**, **2-OAr**, and **1-OAr**. Standard deviations of data are provided.

with increasing number of guanidinate ligands in both the guanidinate−amide mixed-ligand series (from 0.03 for **1-N** to 0.46 for **2-N**, 0.79 for **3-N**, and 0.81 for **4**) and the guanidinate−aryloxide mixed-ligand series (from 0.18 for **1-OAr** to 0.24 for **2-OAr**, 0.32 for **3-OAr**, and 0.81 for **4**). For both series, the quantum yields reached maxima at 0.81 for the blue-emitting complex **4**. This quantum yield was higher than the reported quantum yield of 0.55 in ethanol for the single other blue-emitting Ce^{III} complex, $[Ce^{III}(triRNTB)_2](CF_3SO_3)_3$ complex (triRNTB = tris(*N*-propylbenzimidazol-2-ylmethyl)amine).[58] On the other hand, the low quantum yield of 0.03 for **1-N** indicated the presence of severe nonradiative relaxation processes that quenched the long-lived ^{2}D excited state.

Time-resolved luminescence data were collected near the emission maxima upon excitation at 380 nm (Figures S60−S68). Single exponential fits were applied to the decay data to afford lifetimes (τ). The lifetime for the ^{2}D excited state of **1-N** was found to be shorter (τ = 24 ns) compared to **2-N** (τ = 65 ns), **3-N** (τ = 117 ns), and **4** (τ = 83 ns). These data are within the range of reported lifetimes for molecular Ce^{III} emitters.[54] The difference in lifetime was attributable to the nonradiative decay processes imposed by ligand oscillators. The ability of X−H (*x* = C, N, O, B) oscillators to quench lanthanide long-lived excited states had been widely established in the literature.[75−80] With the partial replacement of amide ligands for guanidinate ligands, the quenching processes from low energy ligand vibrational modes were suppressed. This phenomenon was reflected in the nonradiative decay rates (k_{nr}) extracted from the photoluminescence quantum yields and lifetimes (Table 1); k_{nr} was determined to be 41.0(1) × 10^6

Table 1. Predicted Radiative Decay Rates k_r^{SB} from Strickler−Berg Analysis and Observed Radiative Decay Rates k_r^{obs} and Nonradiative Decay Rates k_{nr}^{obs}

	k_r^{SB} (×10^6 s^{-1})[a]	k_r^{obs} (×10^6 s^{-1})[b]	k_{nr}^{obs} (×10^6 s^{-1})[b]
1-N	1.7	1.12(1)	41.0(1)
2-N	1.7	7.0(1)	8.3(1)
3-N	1.8	6.8(2)	1.8(2)
4	2.4	9.7(3)	2.4(3)
3-OAr	1.7	2.8(1)	5.8(1)
2-OAr	2.1	2.8(1)	8.9(1)
1-OAr	2.7	2.0(1)	9.0(1)

[a] k_r^{SB} was calculated from Strickler−Berg equation. [b] k_r^{obs} and k_{nr}^{obs} were obtained from the equations $k_r^{obs} = \Phi_{PL}/\tau$, $k_{nr}^{obs} = (1 - \Phi_{PL})/\tau$.

s^{-1} for **1-N**, larger than the value 8.3(1) × 10^6 s^{-1} determined for **2-N**, and the values of 1.8(2) × 10^6 s^{-1} and 2.4(3) × 10^6 s^{-1} for **3-N** and **4**, respectively. Similarly, a decreasing trend of k_{nr} was also noted for the guanidinate−aryloxide series, ranging from 9.0(1) × 10^6 s^{-1} for **1-OAr** to 8.9(1) × 10^6 s^{-1} for **2-OAr**, 5.8(1) × 10^6 s^{-1} for **3-OAr**, and 2.4(3) × 10^6 s^{-1} for **4**. The decrease in k_{nr} can also be attributed to the suppression of vibrational quenching processes; the pyramidal solid-state structure of **1-OAr**[61] indicates the presence of C−H agostic interactions. The 5-fold smaller k_{nr} value found for **1-OAr** compared to **1-N** can be understood based on differences in the ligands and their sterics.[81,82] For example, the spatial orientation of methyl groups in the OAr^- ligand prohibits C−H bonds from engaging in agostic interactions as efficiently as the $[N(SiMe_3)_2]^-$ ligands. In addition, the trend in observed k_{nr} for the mixed-ligand series is consistent with the expectation from the energy gap law:[83,84] compounds with lower emission energies demonstrate higher nonradiative decay rates (Figures S72 and S73). On the other hand, the observed radiative decay rates, k_r, ranged from 1.12(1) × 10^6 s^{-1} for **1-N** to 9.7(3) × 10^6 s^{-1} for **4**. The magnitudes of k_r values were consistent with

DOI: 10.1021/jacs.6b02248
J. Am. Chem. Soc. 2016, 138, 5984−5993

predictions made from the Strickler–Berg equation[85] (Table 1, also see Supporting Information).

As with **4**, the pale yellow dimeric complex, **3-I**, was found to be blue emitting, with a quantum yield of 0.53 and a lifetime of 69 ns in toluene. The colorless complex **1-NCl**$^-$ emitted blue light under UV light with a quantum yield of 0.80 and a lifetime of 76 ns. The small Stokes shift (38 nm for **3-I**, 88 nm for **1-NCl**$^-$), high quantum yield, and long lifetime of **3-I** and **1-NCl**$^-$ further support our thesis about the role of vibrational relaxation processes in these luminescent Ce^{III} complexes. With the above photophysical interpretation of Ce^{III} long-lived excited states obtained from spectroscopic and computational results, we were prompted to investigate the photochemical properties for the guanidinate–amide mixed-ligand series.

2.3. Photoinduced Inner and Outer Sphere Electron Transfer. In our previous work, we demonstrated that the ^{2}D excited state of **1-N** and **2-N** could effectively participate in chemical reactions through single electron transfer (SET).[46] The presence of an accessible coordination site in **1-N** and **2-N** allowed inner sphere halogen abstraction reactivity. In this work, the decrease of observed Stokes shifts from 138 nm for **1-N** to 35 nm for **4** implied less energy loss in the excited state of complex **4** compared to **1-N**, affording more powerful photoreductants. On the other hand, the steric congestion around the Ce^{3+} cation in **4** was increased compared to **1-N**, making Ce^{3+} center less accessible for substrates.

In order to estimate the excited-state reduction potentials ($E_{1/2}$) for **3-N** and **4**, the Rehm–Weller formalism was used:[18,86]

$$E_{1/2}^{*} = E_{1/2} - E_{0,0} + \omega$$

In this relationship, the energy difference between zeroth vibrational electronic ground state and excited state ($E_{0,0}$) can be approximated by the emission band energy. The electrostatic interaction due to the separation of charges is represented by the work function, ω. The work function is a small contribution compared to $E_{0,0}$ and usually omitted from the equation for simplicity.[18] The ground-state reduction potential ($E_{1/2}$) was obtained from electrochemistry data collected in CH_2Cl_2.

Cyclic voltammetry of **2-N**, **3-N**, and **4** in CH_2Cl_2 demonstrated quasi-reversible redox features (Figure 6). The observed large separations between the cathodic and anodic waves were intrinsic to the compounds and attributed to slow heterogeneous electron transfer kinetics between the electrodes and solution species.[87,88] To better establish their thermodynamic potentials, the cyclic voltammograms were simulated using reversible $Ce^{III/IV}$ couples ($E_{1/2}$) and standard heterogeneous electron transfer rates (Figure S32). The simulated potentials of the $Ce^{III/IV}$ couples ($E_{1/2}$) for **2-N**, **3-N**, and **4** were determined at +0.09, −0.15, and −0.22 V versus $Cp_2Fe^{0/+}$, respectively. The decreasing $E_{1/2}$ from **2-N** to **4** indicated that guanidinate ligand was more electron donating than the amide ligand. In the case of **1-N**, no feature was observed in CH_2Cl_2. Electrochemical data for **1-N** obtained from THF[89] were applied for the estimation of $E_{1/2}$*, after correcting for the potential difference between those solvents with $Cp_2Fe^{0/+}$ couple.

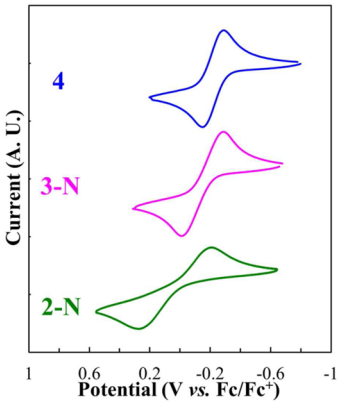

Figure 6. Cyclic voltammetry of **2-N**, **3-N**, and **4** at a scan rate of 0.5 V s^{-1} in CH_2Cl_2, with 0.1 M [^{n}Pr$_4$N][BAr$^F_4$] supporting electrolyte.

Thus, the excited-state reduction potentials $E_{1/2}$* were estimated to be −2.19, −2.30, −2.59, and −2.92 V for complexes **1-N**, **2-N**, **3-N**, and **4**, respectively (Table 2). These results put complex **4** among the strongest known photoreductants, comparable to [(PNP)Cu^I]$_2$ (PNP$^-$ = bis(2-(diisobutylphosphino)phenyl)amide)[32] with its estimated $E_{1/2*}$ of −3.2 V versus $Cp_2Fe^{0/+}$ and W(CNIph)$_6$ (Iph = 2,6-diisopropylphenyl)[22] with an $E_{1/2*}$ of −2.8 V versus $Cp_2Fe^{0/+}$. The guanidinate–amide series complexes are much more reducing than [Ru(bpy)$_3$]$^{2+}$ (bpy =2,2′-bipyridine) and Ir(ppy)$_3$ (ppy =2,2′-phenylpyridine) with values of $E_{1/2*}$ = −1.31 V and −2.23 V versus $Cp_2Fe^{0/+}$, respectively.[7]

Table 2. Estimation of $Ce^{III/IV}$ Reduction Potential in the ^{2}D Excited State for 1-N, 2-N, 3-N, and 4

	$E_{1/2}$[a]/eV	$E_{0,0}$/eV	$E_{1/2}$*/eV
1-N	+0.05[b]	+2.24	−2.19
2-N	+0.09[c]	+2.39	−2.30
3-N	−0.15[c]	+2.44	−2.59
4	−0.22[c]	+2.70	−2.92

[a]Cyclic voltammetry in 0.1 M [^{n}Pr$_4$N][BAr$^F_4$]/CH_2Cl_2. [b]No features observed for **1-N** in CH_2Cl_2; $E_{1/2}$ of **1-N** in THF was used and corrected for the difference of $Cp_2Fe^{0/+}$ in THF and CH_2Cl_2. [c]The quasi-reversible cyclic voltammetry spectra were simulated with $Ce^{III/IV}$ couple ($E_{1/2}$) and heterogeneous electron transfer rates.

Previously, we demonstrated the inner sphere halogen abstraction reactivity of benzyl chloride for **1-N** and **2-N** in their ^{2}D excited states. Irradiating C_6D_6 solutions of **1-N** or **2-N** with excess $PhCH_2Cl$ using commercially available compact fluorescent lamps (CFLs) led to the formation of corresponding Ce^{IV}–Cl compounds, **1-NCl** and **2-NCl**, accompanied by the formation of $PhCH_2CH_2Ph$ (Scheme 2).

In the current work, complexes **3-N** and **4** were more readily oxidized than **1-N** and **2-N** in their ground state. The smaller Stokes shifts of **3-N** and **4** compared to **1-N** and **2-N** indicate less energy losses for **3-N** and **4** in their excited states following vertical transitions at ca. 420 nm. However, no reaction was observed for **3-N** or **4** with $PhCH_2Cl$ under the same reaction conditions (Figures S22 and S23). The lack of reactivity for **3-N** and **4** toward $PhCH_2Cl$ can be rationalized based on the accessibility of the Ce^{3+} cation; the steric congestion in **3-N** and **4** around the Ce^{3+} cations does not favor substrate association in their ^{2}D excited states.

We have also demonstrated the photocatalytic coupling reactions between 4-F-C_6H_4X (x = Br, I) and benzene mediated by **1-N** to afford 1-(4-fluorophenyl)benzene.[46] In addition to the observation of corresponding Ce^{IV}–Br species in stoichiometric reactions between **1-N** and 1-bromo-4-fluorobenzene,[46] the inner sphere SET mechanism of **1-N**

DOI: 10.1021/jacs.6b02248
J. Am. Chem. Soc. 2016, 138, 5984–5993

Scheme 2. Reaction of 1-N, 2-N, 3-N, and 4 with Excess $PhCH_2Cl$ in C_6D_6 under Compact Fluorescent Lamp Irradiation

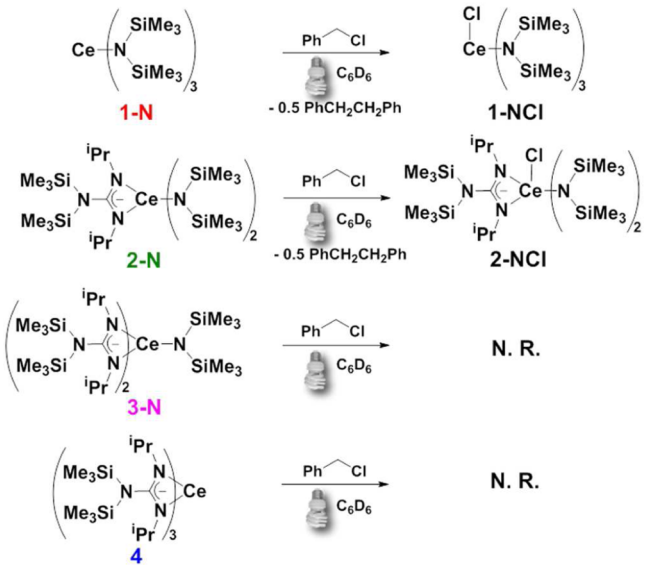

with aryl bromides is also reflected in the relative conversions of catalytic reactions toward different *para*-substituted substrates (Table 3). The conversion of 4-R-C_6H_4Br (R = Me, H, F) was found to decrease with the electron donating ability of the substituents under same reaction conditions (entry 1−3). Such a pattern of reactivity is opposite to that expected for an outer sphere SET mechanism where electron poor aryl rings would be more efficient electron acceptors. Rather, the observed Me > H > F sequence is consistent with an inner sphere SET pathway where more electron-rich aryl bromide associates with Ce^{3+} cation more readily. Interestingly, 2-fluorophenyl bromide reacts much faster and reaches complete conversion under the same reaction conditions (entry 4). We tentatively attributed this result to the chelation effect of 2-fluorophenyl bromide to the Ce^{3+} cation through C−F→Ce^{III} interaction[90−95] that facilitated substrate binding to the Ce^{3+} cation. The involvement of C−F→Ln^{III} (Ln = La, Sm, Yb) interactions has also been postulated for stoichiometric and catalytic functionalization of C−F bonds mediated by lanthanide complexes.[96−98]

Table 3. Catalytic Photoinduced Arylation Reactions of Benzene Mediated by 1-N

entry	X	R	conversion[a]/%	yield[a]/%
1	Br	4-Me	92	76
2	Br	H	80	72
3	Br	4-F	69	32
4	Br	2-F	>99	86
5	I	4-Me	>99	76
6	I	H	>99	85
7	I	4-F	>99	91
8	I	2-F	>99	87
9	I	3-Me	>99	88
10	I	2-Me	>99	23

[a]All percentage conversions to product (percentage conversions of aryl halide starting materials) are determined by GC.

The arylation reaction of benzene catalyzed by **1-N** was found to be faster for aryl iodides compared to aryl bromides; quantitative conversion can be achieved for aryl iodides (entries 5−10) under the same reaction conditions for aryl bromides. Notably, a significantly lower yield was observed for 2-methylphenyl iodide (entry 10, 23%) compared to 4-methylphenyl iodide (entry 5, 76%) and 3-methylphenyl iodide (entry 9, 88%), despite the complete conversion for all three substrates. This observation can also be reasoned based on our proposed reaction pathway (Scheme 4A); direct H atom abstraction of bulky $^{\bullet}N(SiMe_3)_2$ radical from radical adduct $[Ar-C_6H_6]^{\bullet}$ is expected to be unfavorable for the 2-methylphenyl iodide substrate.

Scheme 3. Catalytic Photoinduced Phenylation of 4-Fluorophenyl Iodide with 4

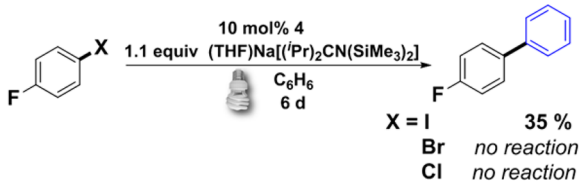

Scheme 4. Proposed Cycle for Photoinduced Arylation of Benzene through Inner Sphere SET Pathway and Outer Sphere SET Pathway

A. Inner sphere SET pathway with 1-N (X = Br, I):

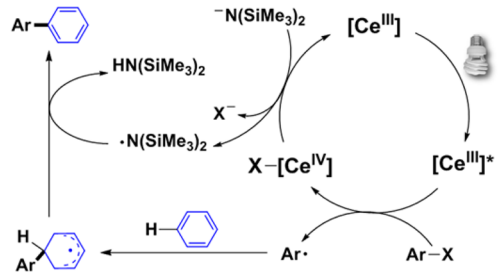

B. Outer sphere SET pathway with 4 (X = I):

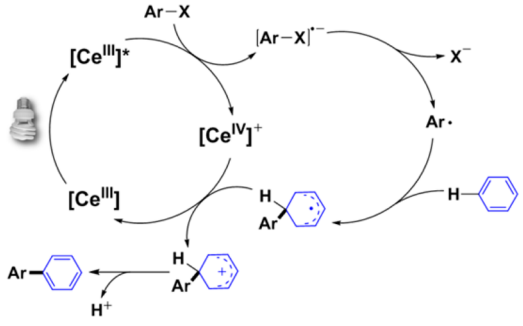

We also investigated phenylation reactions of aryl halides with complex **4**. Such reactions using 4-F-C_6H_4X (*x* = Br, I) and stoichiometric amount of $NaN(SiMe_3)_2$ in benzene with **1-N** as photoredox catalyst had been shown by us to afford 1-(4-fluorophenyl)benzene by an inner sphere halogen abstraction pathway.[46] In this case, irradiation of a benzene solution containing 4-fluoroiodobenzene, $(THF)Na[(N^iPr)_2CN(SiMe_3)_2]$, and 10 mol% **4** for 6 days led to the isolation of 1-(4-fluorophenyl)benzene in 35% yield (Scheme 3) while no reactions were observed for the 4-F-C_6H_4Br and 4-F-C_6H_4Cl

DOI: 10.1021/jacs.6b02248
J. Am. Chem. Soc. 2016, 138, 5984−5993

substrates. The phenylation reaction of 4-fluoroiodobenzene mediated by **4** was also performed with intermittent light (Figure S84); no 1-(4-fluorophenyl)benzene formation was observed during the dark period, suggesting that the product formation likely did not involve a radical propagation process.

To further elucidate the difference in interactions of Ce^{III} complexes with substrates, quenching kinetic data were obtained for **1-N**, **2-N**, **3-N**, and **4** through Stern−Volmer experiments[99] using 4-fluoroiodobenzene as a quencher. The calculated quenching rate, k_q, was found to be $3.5(1) \times 10^7$ M^{-1} s^{-1} for **4**, 2 orders of magnitude smaller than $2.12(2) \times 10^9$ M^{-1} s^{-1} calculated for **1-N** (Table 4). The smaller quenching rate for **4** was attributed to the steric encumbrance around the Ce^{3+} cation, preventing its direct interaction with aryl iodide substrates.

Table 4. Quenching Rates of 1-N, 2-N, 3-N, and 4 with 4-Fluoroiodobenzene as Quencher

	1-N	2-N	3-N	4
k_q ($\times 10^8$ M^{-1} s^{-1})	21.2(2)	2.18(3)	0.19(1)	0.35(1)

In addition, we also noted that complex **4** was incapable of associating a Cl^- anion (Figure S28) or reacting with an inner sphere oxidant Ph_3C-Cl (Figure S29). In contrast, complex **1-N** reacts readily with NEt_4Cl to form $[NEt_4]\{Ce^{III}Cl[N(SiMe_3)_2]_3\}$ (**1-NCl**$^-$) and with Ph_3C-Cl to afford $Ce^{IV}Cl[N(SiMe_3)_2]_3$ (**1-NCl**). These differences in reactivity between **1-N** and **4** suggest that the steric encumbrance around the Ce^{3+} cation in **4** was sufficiently large to prevent substrate binding. Considering the differences in quenching kinetics and reactivity, we are prompted to propose that the single electron transfer of **4** occurs through an outer sphere pathway instead of an inner sphere pathway. Therefore, the catalytic cycle for the phenylation of aryl iodide with **4** would comprise the following steps (Scheme 4B): (1) photoinduced reduction of 4-F-C_6H_4I by **4** to produce $\mathbf{4}^+$ and $[4\text{-F-}C_6H_4I]^{\bullet-}$; (2) dissociation of the radical anion to give iodide and 4-F-$C_6H_4^{\bullet}$; (3) addition of 4-F-$C_6H_4^{\bullet}$ to benzene forming a radical adduct; (4) oxidation of the radical adduct by $\mathbf{4}^+$ to regenerate **4**; (5) reaction of $(THF)Na[(N^iPr)_2CN(SiMe_3)_2]$ with H^+ to afford the biphenyl product. Similar outer sphere single electron transfer pathways for catalytic phenylation reactions of aryl halides have been reported with group I and transition metal 1,10-phenanthroline complexes at elevated temperatures.[100−104] More recently, homolytic aromatic substitution reactions mediated by the photoredox catalyst $Ir(ppy)_3$ have also been demonstrated.[14]

The one-electron oxidation product of **4** was synthesized. Treatment of **4** with $[Cp_2Fe][BAr^F{}_4]$ in THF followed by recrystallization from CH_2Cl_2/*n*-pentane layering afforded dark green crystals of $[\mathbf{4}^+][BAr^F{}_4]$. An X-ray diffraction study of $[\mathbf{4}^+][BAr^F{}_4]$ confirmed the proposed cationic tris-guanidinate structure with average Ce−N bond length observed at 2.397(4) Å for $\mathbf{4}^+$, compared to 2.526(4) Å observed for **4** (Figure S7). The ca. 0.1 Å difference in Ce−N bond lengths was consistent with the difference in ionic radii between Ce^{3+} and Ce^{4+} cations.[105] The dark green color of $\mathbf{4}^+$ cation is uncommon for Ce^{IV} compounds.[106] A UV−vis spectrum of $[\mathbf{4}^+][BAr^F{}_4]$ collected in CH_2Cl_2 revealed an intriguingly low energy absorption band at 1.60 eV (775 nm, Figure S41), indicative of small HOMO−LUMO gap.[46,107] This LMCT band was tentatively assigned to a transition from the guanidinate nonbonding π orbitals (π_n) to a cerium 4f orbital. The isolation of $[\mathbf{4}^+]$ suggests that the outer sphere single electron transfer of **4** is a viable process.

3. CONCLUSIONS

We have demonstrated, through comparison studies on two complete mixed-ligand series, that vibrational relaxation process played a key role in Ce^{III} luminescence. The ^2D excited states, with singly occupied $5d_{z^2}$ orbital, were determined, using a combination of TD-DFT and spectroscopic studies, to be the long-lived excited state for the luminescent Ce^{III} complexes, in approximate C_{2v} or C_{3v} geometries. Although essentially the same energy of light (ca. 420 nm, 2.95 eV) is required to promote the vertical absorptive transitions for these complexes to their lowest energy ^2D excited states, drastically different emission energies (from 553 nm, 2.24 eV to 459 nm, 2.70 eV) were found for the complexes. Such energy variance reflected in the Stokes shifts indicates different degrees of vibrational relaxation associated with the local ligand environments. The long-lived excited state also suffered from vibrational quenching processes, leading to various lifetimes and quantum yields of the complexes.

In terms of rational Ce^{III} photosensitizer design, we propose that the relaxation of the excited state should be minimized in order to confer maximum energy from light into chemical transformations or photovoltages. Our studies offer a design strategy for achieving powerful molecular Ce^{III} photoreductants by using rigid ligands as well as removing C−H oscillators from proximity with the metal cation, in order to minimize vibrational relaxation of the excited state. On the other hand, tuning the degree of relaxation and quenching process could afford Ce^{III} luminophores with tunable emission colors and efficiency.

As an expansion to the inner sphere electron transfer reactivity of **1-N** previously reported by us,[46] we demonstrated that complex **4**, with a less accessible metal cation than **1-N**, participated in an outer sphere electron transfer pathway with 4-fluoroiodobenzene to afford 1-(4-fluorophenyl)benzene. These combined results revealed the possibility of using f-block cations as photoredox catalysts. However, the efficiency of these catalytic reactions mediated by Ce^{III} photosensitizers is currently limited by the low absorptivity intrinsic to f → d transitions. Further studies on sensitization of Ce^{III} luminophores are underway to improve their light harvesting capabilities.

■ ASSOCIATED CONTENT

Supporting Information

The Supporting Information is available free of charge on the ACS Publications website at DOI: 10.1021/jacs.6b02248.

Electrochemical, electronic absorption, and excitation and emission data, computational details, and optimization data for catalysis (PDF)

Crystallographic data (CIF)

■ AUTHOR INFORMATION

Corresponding Authors

*jmanna@sas.upenn.edu

*schelter@sas.upenn.edu

Notes

The authors declare no competing financial interest.

DOI: 10.1021/jacs.6b02248
J. Am. Chem. Soc. 2016, 138, 5984−5993

■ ACKNOWLEDGMENTS

We gratefully acknowledge the University of Pennsylvania and the National Science Foundation (CHE-1362854) for financial support. This work used the Extreme Science and Engineering Discovery Environment (XSEDE), which is supported by U.S. National Science Foundation Grant No. OCI-1053575. The E. J. Petersson, D. M. Chenoweth, and S. Park groups at UPenn are thanked for use of their fluorometers. The Walsh group at UPenn is acknowledged for use of their GC.

■ REFERENCES

(1) Gao, F. G.; Bard, A. J. *J. Am. Chem. Soc.* **2000**, *122*, 7426−7427.
(2) Li, J.-C.; Wu, J.-Z.; Gong, X. *J. Phys. Chem. Lett.* **2014**, *5*, 1017−1021.
(3) Hussain, M.; El-Shafei, A.; Islam, A.; Han, L. *Phys. Chem. Chem. Phys.* **2013**, *15*, 8401−8408.
(4) Schultz, D. M.; Yoon, T. P. *Science* **2014**, *343*, 1239176.
(5) Nguyen, J. D.; D'Amato, E. M.; Narayanam, J. M. R.; Stephenson, C. R. J. *Nat. Chem.* **2012**, *4*, 854−859.
(6) Reckenthäler, M.; Griesbeck, A. G. *Adv. Synth. Catal.* **2013**, *355*, 2727−2744.
(7) Koike, T.; Akita, M. *Inorg. Chem. Front.* **2014**, *1*, 562−576.
(8) Zeitler, K. *Angew. Chem., Int. Ed.* **2009**, *48*, 9785−9789.
(9) Yoon, T. P.; Ischay, M. A.; Du, J. *Nat. Chem.* **2010**, *2*, 527−532.
(10) Narayanam, J. M. R.; Stephenson, C. R. J. *Chem. Soc. Rev.* **2011**, *40*, 102−113.
(11) Xuan, J.; Xiao, W.-J. *Angew. Chem., Int. Ed.* **2012**, *51*, 6828−6838.
(12) Maity, S.; Zheng, N. *Synlett* **2012**, *23*, 1851−1856.
(13) Prier, C. K.; Rankic, D. A.; MacMillan, D. W. C. *Chem. Rev.* **2013**, *113*, 5322−5363.
(14) Cheng, Y.; Gu, X.; Li, P. *Org. Lett.* **2013**, *15*, 2664−2667.
(15) Hari, D. P.; König, B. *Angew. Chem., Int. Ed.* **2013**, *52*, 4734−4743.
(16) Hopkinson, M. N.; Sahoo, B.; Li, J.-L.; Glorius, F. *Chem. - Eur. J.* **2014**, *20*, 3874−3886.
(17) Tellis, J. C.; Primer, D. N.; Molander, G. A. *Science* **2014**, *345*, 433−436.
(18) Tucker, J. W.; Stephenson, C. R. J. *J. Org. Chem.* **2012**, *77*, 1617−1622.
(19) Fei, H.; Sampson, M. D.; Lee, Y.; Kubiak, C. P.; Cohen, S. M. *Inorg. Chem.* **2015**, *54*, 6821−6828.
(20) Li, D.; Che, C.-M.; Kwong, H.-L.; Yam, V. W.-W. *J. Chem. Soc., Dalton Trans.* **1992**, 3325−3329.
(21) Revol, G.; McCallum, T.; Morin, M.; Gagosz, F.; Barriault, L. *Angew. Chem., Int. Ed.* **2013**, *52*, 13342−13345.
(22) Sattler, W.; Ener, M. E.; Blakemore, J. D.; Rachford, A. A.; LaBeaume, P. J.; Thackeray, J. W.; Cameron, J. F.; Winkler, J. R.; Gray, H. B. *J. Am. Chem. Soc.* **2013**, *135*, 10614−10617.
(23) Sattler, W.; Henling, L. M.; Winkler, J. R.; Gray, H. B. *J. Am. Chem. Soc.* **2015**, *137*, 1198−1205.
(24) Creutz, S. E.; Lotito, K. J.; Fu, G. C.; Peters, J. C. *Science* **2012**, *338*, 647−651.
(25) Bissember, A. C.; Lundgren, R. J.; Creutz, S. E.; Peters, J. C.; Fu, G. C. *Angew. Chem., Int. Ed.* **2013**, *52*, 5129−5133.
(26) Ziegler, D. T.; Choi, J.; Muñoz-Molina, J. M.; Bissember, A. C.; Peters, J. C.; Fu, G. C. *J. Am. Chem. Soc.* **2013**, *135*, 13107−13112.
(27) Tan, Y.; Munoz-Molina, J. M.; Fu, G. C.; Peters, J. C. *Chem. Sci.* **2014**, *5*, 2831−2835.
(28) Uyeda, C.; Tan, Y.; Fu, G. C.; Peters, J. C. *J. Am. Chem. Soc.* **2013**, *135*, 9548−9552.
(29) Kern, J.-M.; Sauvage, J.-P. *J. Chem. Soc., Chem. Commun.* **1987**, 546−548.
(30) Pirtsch, M.; Paria, S.; Matsuno, T.; Isobe, H.; Reiser, O. *Chem. - Eur. J.* **2012**, *18*, 7336−7340.
(31) Bagal, D. B.; Kachkovskyi, G.; Knorn, M.; Rawner, T.; Bhanage, B. M.; Reiser, O. *Angew. Chem., Int. Ed.* **2015**, *54*, 6999−7002.
(32) Harkins, S. B.; Peters, J. C. *J. Am. Chem. Soc.* **2005**, *127*, 2030−2031.
(33) Miller, A. J. M.; Dempsey, J. L.; Peters, J. C. *Inorg. Chem.* **2007**, *46*, 7244−7246.
(34) Lotito, K. J.; Peters, J. C. *Chem. Commun.* **2010**, *46*, 3690−3692.
(35) Deaton, J. C.; Switalski, S. C.; Kondakov, D. Y.; Young, R. H.; Pawlik, T. D.; Giesen, D. J.; Harkins, S. B.; Miller, A. J. M.; Mickenberg, S. F.; Peters, J. C. *J. Am. Chem. Soc.* **2010**, *132*, 9499−9508.
(36) Xiang, H.; Cheng, J.; Ma, X.; Zhou, X.; Chruma, J. J. *Chem. Soc. Rev.* **2013**, *42*, 6128−6185.
(37) Ghosh, I.; Ghosh, T.; Bardagi, J. I.; König, B. *Science* **2014**, *346*, 725−728.
(38) Thekaekara, M. P. *Sol. Energy* **1976**, *18*, 309−325.
(39) Cotton, S. *Lanthanide and Actinide Chemistry*; John Wiley and Sons: West Sussex, U.K., 2006; pp 61−77.
(40) Aspinall, H. C. *Chemistry of the f-Block Elements*; CRC Press: 2001; p 34.
(41) Duan, C. K.; Reid, M. F. *J. Solid State Chem.* **2003**, *171*, 299−303.
(42) Heidt, L. J.; Smith, M. E. *J. Am. Chem. Soc.* **1948**, *70*, 2476−2481.
(43) Heidt, L. J.; McMillan, A. F. *J. Am. Chem. Soc.* **1954**, *76*, 2135−2139.
(44) Donohue, T. *Chem. Phys. Lett.* **1979**, *61*, 601−604.
(45) Matthews, R. W.; Sworski, T. J. *J. Phys. Chem.* **1975**, *79*, 681−686.
(46) Yin, H.; Carroll, P. J.; Anna, J. M.; Schelter, E. J. *J. Am. Chem. Soc.* **2015**, *137*, 9234−9237.
(47) Russell−Saunders term symbols (^{2}D or ^{2}F) are used in this work to represent the ground and excited states. In our previous communication, we used crystal field states to represent a specific excited state ($^2A_1$) based on 5d orbital splittings under C_{2v} and C_{3v} crystal fields.
(48) Haxel, G. B.; Hedrick, J. B.; Orris, G. J. *Rare Earth Elements—Critical Resources for High Technology*; U.S. Geological Survey: 2002.
(49) Mioduski, T.; Hao, D.; Luan, H. *J. Radioanal. Nucl. Chem.* **1989**, *132*, 105−113.
(50) George, N. C.; Denault, K. A.; Seshadri, R. *Annu. Rev. Mater. Res.* **2013**, *43*, 481−501.
(51) Blasse, G.; Bril, A. *Appl. Phys. Lett.* **1967**, *11*, 53−55.
(52) Hazin, P. N.; Bruno, J. W.; Brittain, H. G. *Organometallics* **1987**, *6*, 913−918.
(53) Rausch, M. D.; Moriarty, K. J.; Atwood, J. L.; Weeks, J. A.; Hunter, W. E.; Brittain, H. G. *Organometallics* **1986**, *5*, 1281−1283.
(54) Hazin, P. N.; Lakshminarayan, C.; Brinen, L. S.; Knee, J. L.; Bruno, J. W.; Streib, W. E.; Folting, K. *Inorg. Chem.* **1988**, *27*, 1393−1400.
(55) Kunkely, H.; Vogler, A. *J. Photochem. Photobiol., A* **2002**, *151*, 45−47.
(56) Jiao, Y.; Wang, J.; Wu, P.; Zhao, L.; He, C.; Zhang, J.; Duan, C. *Chem. - Eur. J.* **2014**, *20*, 2224−2231.
(57) Zhao, L.; Liu, Y.; He, C.; Wang, J.; Duan, C. *Dalton Trans.* **2014**, *43*, 335−343.
(58) Zheng, X.-L.; Liu, Y.; Pan, M.; Lü, X.-Q.; Zhang, J.-Y.; Zhao, C.-Y.; Tong, Y.-X.; Su, C.-Y. *Angew. Chem., Int. Ed.* **2007**, *46*, 7399−7403.
(59) Vogler, A.; Kunkely, H. *Inorg. Chim. Acta* **2006**, *359*, 4130−4138.
(60) Steele, L. A. M.; Boyle, T. J.; Kemp, R. A.; Moore, C. *Polyhedron* **2012**, *42*, 258−264.
(61) Stecher, H. A.; Sen, A.; Rheingold, A. L. *Inorg. Chem.* **1988**, *27*, 1130−1132.
(62) Higashiyama, N.; Takemura, K.; Kimura, K.; Adachi, G.-y. *Inorg. Chim. Acta* **1992**, *194*, 201−206.
(63) Kuda-Wedagedara, A. N. W.; Wang, C.; Martin, P. D.; Allen, M. J. *J. Am. Chem. Soc.* **2015**, *137*, 4960−4963.
(64) Tretiak, S.; Saxena, A.; Martin, R. L.; Bishop, A. R. *Chem. Phys. Lett.* **2000**, *331*, 561−568.
(65) Martin, R. L. *J. Chem. Phys.* **2003**, *118*, 4775−4777.

DOI: 10.1021/jacs.6b02248
J. Am. Chem. Soc. 2016, 138, 5984−5993

(66) Atwood, D. A. *The Rare Earth Elements: Fundamentals and Applications*; Wiley: 2013; pp 27−34.
(67) Rogers, E. G.; Dorenbos, P. *J. Lumin.* **2014**, *155*, 135−140.
(68) Langeslay, R. R.; Fieser, M. E.; Ziller, J. W.; Furche, F.; Evans, W. J. *Chem. Sci.* **2015**, *6*, 517−521.
(69) Hitchcock, P. B.; Lappert, M. F.; Maron, L.; Protchenko, A. V. *Angew. Chem., Int. Ed.* **2008**, *47*, 1488−1491.
(70) MacDonald, M. R.; Bates, J. E.; Ziller, J. W.; Furche, F.; Evans, W. J. *J. Am. Chem. Soc.* **2013**, *135*, 9857−9868.
(71) MacDonald, M. R.; Fieser, M. E.; Bates, J. E.; Ziller, J. W.; Furche, F.; Evans, W. J. *J. Am. Chem. Soc.* **2013**, *135*, 13310−13313.
(72) Fjeldberg, T.; Andersen, R. A. *J. Mol. Struct.* **1985**, *129*, 93−105.
(73) Williams, A. T. R.; Winfield, S. A.; Miller, J. N. *Analyst* **1983**, *108*, 1067−1071.
(74) Suzuki, K.; Kobayashi, A.; Kaneko, S.; Takehira, K.; Yoshihara, T.; Ishida, H.; Shiina, Y.; Oishi, S.; Tobita, S. *Phys. Chem. Chem. Phys.* **2009**, *11*, 9850−9860.
(75) Browne, W. R.; Vos, J. G. *Coord. Chem. Rev.* **2001**, *219−221*, 761−787.
(76) Bunzli, J.-C. G.; Piguet, C. *Chem. Soc. Rev.* **2005**, *34*, 1048−1077.
(77) Marks, S.; Heck, J. G.; Habicht, M. H.; Oña-Burgos, P.; Feldmann, C.; Roesky, P. W. *J. Am. Chem. Soc.* **2012**, *134*, 16983−16986.
(78) Bünzli, J.-C. G. *Coord. Chem. Rev.* **2015**, *293−294*, 19−47.
(79) Yanagida, S.; Hasegawa, Y.; Murakoshi, K.; Wada, Y.; Nakashima, N.; Yamanaka, T. *Coord. Chem. Rev.* **1998**, *171*, 461−480.
(80) Doffek, C.; Seitz, M. *Angew. Chem., Int. Ed.* **2015**, *54*, 9719−9721.
(81) Edelmann, F. T. *Chem. Soc. Rev.* **2012**, *41*, 7657−7672.
(82) Edelmann, F. T. *Chem. Soc. Rev.* **2009**, *38*, 2253−2268.
(83) Griesser, H. J.; Wild, U. P. *Chem. Phys.* **1980**, *52*, 117−131.
(84) Kober, E. M.; Caspar, J. V.; Lumpkin, R. S.; Meyer, T. J. *J. Phys. Chem.* **1986**, *90*, 3722−3734.
(85) Strickler, S. J.; Berg, R. A. *J. Chem. Phys.* **1962**, *37*, 814−822.
(86) Rehm, D.; Weller, A. *Isr. J. Chem.* **1970**, *8*, 259−271.
(87) Robinson, J. R.; Gordon, Z.; Booth, C. H.; Carroll, P. J.; Walsh, P. J.; Schelter, E. J. *J. Am. Chem. Soc.* **2013**, *135*, 19016−19024.
(88) Robinson, J. R.; Carroll, P. J.; Walsh, P. J.; Schelter, E. J. *Angew. Chem., Int. Ed.* **2012**, *51*, 10159−10163.
(89) Williams, U. J.; Robinson, J. R.; Lewis, A. J.; Carroll, P. J.; Walsh, P. J.; Schelter, E. J. *Inorg. Chem.* **2014**, *53*, 27−29.
(90) Plenio, H. *Chem. Rev.* **1997**, *97*, 3363−3384.
(91) Lewis, A. J.; Yin, H.; Carroll, P. J.; Schelter, E. J. *Dalton Trans.* **2014**, *43*, 10844−10851.
(92) Yin, H.; Robinson, J. R.; Carroll, P. J.; Walsh, P. J.; Schelter, E. J. *Chem. Commun.* **2014**, *50*, 3470−3472.
(93) Yin, H.; Lewis, A. J.; Carroll, P.; Schelter, E. J. *Inorg. Chem.* **2013**, *52*, 8234−8243.
(94) Yin, H.; Lewis, A. J.; Williams, U. J.; Carroll, P. J.; Schelter, E. J. *Chem. Sci.* **2013**, *4*, 798−805.
(95) Yin, H.; Zabula, A. V.; Schelter, E. J. *Dalton Trans.* **2016**, *45*, 6313−6323.
(96) Janjetovic, M.; Träff, A. M.; Hilmersson, G. *Chem. - Eur. J.* **2015**, *21*, 3772−3777.
(97) Träff, A. M.; Janjetovic, M.; Ta, L.; Hilmersson, G. *Angew. Chem., Int. Ed.* **2013**, *52*, 12073−12076.
(98) Janjetovic, M.; Traff, A. M.; Ankner, T.; Wettergren, J.; Hilmersson, G. *Chem. Commun.* **2013**, *49*, 1826−1828.
(99) Lakowicz, J. R. *Principles of Fluorescence Spectroscopy*; Springer: 2007; pp 54−55.
(100) Shirakawa, E.; Itoh, K.-i.; Higashino, T.; Hayashi, T. *J. Am. Chem. Soc.* **2010**, *132*, 15537−15539.
(101) Li, H.; Sun, C.-L.; Yu, M.; Yu, D.-G.; Li, B.-J.; Shi, Z.-J. *Chem. - Eur. J.* **2011**, *17*, 3593−3597.
(102) Sun, C.-L.; Li, H.; Yu, D.-G.; Yu, M.; Zhou, X.; Lu, X.-Y.; Huang, K.; Zheng, S.-F.; Li, B.-J.; Shi, Z.-J. *Nat. Chem.* **2010**, *2*, 1044−1049.
(103) Sun, C.-L.; Gu, Y.-F.; Huang, W.-P.; Shi, Z.-J. *Chem. Commun.* **2011**, *47*, 9813−9815.
(104) Liu, W.; Cao, H.; Zhang, H.; Zhang, H.; Chung, K. H.; He, C.; Wang, H.; Kwong, F. Y.; Lei, A. *J. Am. Chem. Soc.* **2010**, *132*, 16737−16740.
(105) Shannon, R. *Acta Crystallogr., Sect. A: Cryst. Phys., Diffr., Theor. Gen. Crystallogr.* **1976**, *32*, 751−767.
(106) Piro, N. A.; Robinson, J. R.; Walsh, P. J.; Schelter, E. J. *Coord. Chem. Rev.* **2014**, *260*, 21−36.
(107) Walter, M. D.; Booth, C. H.; Lukens, W. W.; Andersen, R. A. *Organometallics* **2009**, *28*, 698−707.

DOI: 10.1021/jacs.6b02248
J. Am. Chem. Soc. 2016, 138, 5984−5993